[UCI]I804:48009-200000171668

의학박사 학위논문

염증성 장질환의 마우스 모델에서의 xC^- 수송체 활성도를 영상화하기 위한 [^{18}F]FSPG-PET를 이용한 전임상실험

Exploratory preclinical investigation of (4S)-4-(3-^{18}F-fluoropropyl)-L-glutamate positron emission tomography for imaging x_C^- transporter activity in murine models of inflammatory bowel disease

울산대학교대학원
의 학 과
서민정

Exploratory preclinical investigation of (4S)-4-(3-^{18}F-fluoropropyl)-L-glutamate positron emission tomography for imaging x_C^- transporter activity in murine models of inflammatory bowel disease

지 도 교 수　　문대혁

이 논문을 의학박사 학위 논문으로 제출함

2018 년 12 월

울 산 대 학 교 대 학 원

의　학　과

서민정

서민정의 의학박사학위 논문을 인준함

심사위원 류진숙 인

심사위원 문대혁 인

심사위원 예병덕 인

심사위원 권미나 인

심사위원 김지영 인

울 산 대 학 교 대 학 원

2018 년 12 월

Abstract

Purpose: The present study assessed the feasibility of (4S)-4-(3-^{18}F-fluoropropyl)-L-glutamate positron emission tomography/magnetic resonance imaging ([^{18}F]FSPG PET/MRI) for detecting inflammation in murine models of colitis.

Methods: Two murine models of colitis were developed by administrating dextran sodium sulfate (DSS) or transferring T cells. Both [^{18}F]FSPG and [^{18}F]fluorodeoxyglucose (FDG) PET/MRI scans were obtained at the time of colitis development. The disease activity index (DAI), pathologic score, and standardized uptake (SUV) were calculated. Immunohistochemical (IHC) expression levels of xCT, Glut1, and immune cell markers (CD11c, F4/80, CD3, and B220) were analyzed.

Results: A total of 12 and 11 mice developed DSS-induced colitis and T cell-transferred colitis, respectively. Both groups of mice showed significantly increased [^{18}F]FSPG uptake

in the colon compared to controls, with higher uptake in T cell-transferred mice. [^{18}F]FDG SUV was higher than [^{18}F]FSPG SUV in T cell-transferred mice but not in DSS-treated mice. [^{18}F]FSPG and [^{18}F]FDG uptakes both showed positive correlations with disease severity (DAI and pathologic score) in both murine models. IHC staining showed significant expression of xCT and Glut1 in the epithelium and lamina propria. A proportion of CD11c^{+} dendritic cells, F4/80^{+} macrophages, and CD3^{+} T cells co-expressed xCT and Glut1 in both models of colitis, with a higher proportion in T cell-transferred mice.

Conclusion: [^{18}F]FSPG PET is a useful means of evaluating murine models of colitis. Its uptake is positively correlated with clinical and histological markers of disease activity. Further studies are needed to assess its utility in evaluating human inflammatory bowel disease.

Key Words: [^{18}F]FSPG, positron emission tomography, inflammatory bowel disease,

colitis

Contents

Abstract ····· i

List of figures ····· v

List of tables ····· vii

Introduction ····· 1

Materials and methods ····· 11

Results ····· 22

Discussion ····· 29

Conclusion ····· 35

References ····· 36

국문요약 ····· 62

List of figures

Figure 1.

Development of a dextran sodium sulfate (DSS)-induced colitis model. ····· 44

Figure 2.

Development of a T cell-transferred colitis model. ····· 46

Figure 3.

[^{18}F]FDG and [^{18}F]FSPG PET/MRI images of dextran sodium sulfate-treated mice. ···· 48

Figure 4.

[^{18}F]FDG and [^{18}F]FSPG PET/MRI images of T cell-transferred mice. ····· 49

Figure 5.

Confocal microscopic images of the middle colon from dextran sodium sulfate-treated mice and BALB/c wild-type mice. ····· 50

Figure 6.

Confocal microscopic images of the proximal, middle, and distal colon from dextran sodium sulfate-treated mice. ····· 52

Figure 7.

Confocal microscopic images showing cells with co-expressions in the colon from dextran sodium sulfate-treated mice. ····· 54

Figure 8.

Confocal microscopic images of the middle colon from $CD4^{+}CD45RB^{high}$ T cell-transferred mice and $Rag2^{-/-}\gamma c^{-/-}$ mice. ····· 55

Figure 9.
Confocal microscopic images of the proximal, middle, and distal colon from T cell-transferred mice. ····· 57

Figure 10.
Confocal microscopic images showing cells with co-expressions in the colon from T cell-transferred mice. ····· 59

List of tables

Table 1.

Dextran sodium sulfate (DSS)-treated mice and their controls: Colitis severity and PET findings ····· 60

Table 2.

T cell-transferred mice and their controls: Colitis severity and PET findings ····· 61

Introduction

Inflammatory bowel disease (IBD) represents a group of inflammatory conditions of the colon and small intestine, among which ulcerative colitis (UC) and Crohn's disease (CD) are principal types, with both overlapping and distinct clinical and pathological features[1, 2]. IBD is prevalent worldwide and both its incidence and prevalence are increasing[1, 3, 4]. As a chronic relapsing condition without a permanent drug therapy, it can be debilitating[5], with life-threatening complications, and is reported to be associated with significant morbidity, comorbidity, and mortality[6]. Despite recent advances, up to 80% of CD patients must undergo at least one surgical removal. In CD, disease activity has a huge impact on quality of life and up to 10-15% of affected individuals ultimately need a colectomy[7]. Although there are few comprehensive studies of IBD comorbidity, IBD is known to be associated with multiple diseases, such as certain cancers, osteoporosis, and psychological disorders[8-11]. Despite similar causes of death in UC and CD, there seem to be differences in cause-specific mortality. While conventional causes of death such as malignancy do not seem to be as significant as originally noted, emerging threats such as infection should be paid attention[6].

Due to the significant morbidity and mortality of IBD, considerable research is currently underway focusing on its pathogenesis and on factors triggering flares. During the onset and reactivation of IBD, there is a heightened immune response to microbial flora in which inflammatory mediators migrate to target organs, resulting in an influx of inflammatory cells, including overly aggressive T cells[12]. This trafficking of lymphocytes requires a multi-step adhesion cascade mediated by adhesion molecules and integrin molecules, some of which are targets for novel drugs and imaging[2, 13-17]. The accumulation of excess lymphocytes in the intestinal lamina propria is a hallmark of IBD pathogenesis[2, 18], and this sustained recruitment of inflammatory T cells ultimately results in tissue damage. UC and CD are characterized by very different T cell responses. Traditionally, Th1 (related to the chronicity of inflammation) cells have been thought to play an important role in the pathogenesis of CD while a Th2-like response is the major response in UC. Recent studies report that a newly described set of T helper cells, the Th17 cells, are significantly infiltrated in both UC and CD and that there is an imbalance in Th17/T-regulatory cells[19-22]. Innate immune cells, such as dendritic cells, are also over-activated in IBD[23].

Various therapies have been introduced to treat the various clinical manifestations and complications of IBD, but for several decades, medical treatments were limited to non-biological therapies, which may provide symptomatic relief but do not change the disease course[24]. Increased understanding of the immunopathology has led to the development of targeted therapies beyond anti-tumor necrosis factor agents, including agents that target adhesion molecules, such as intracellular cell adhesion molecule (ICAM)-1, ICAM-2, vascular cell adhesion molecule-1 (VCAM-1), and mucosal vascular addressin cell adhesion molecule 1 (MAdCAM-1)[2]. However, these treatments have not been effective in all patients and many are still in the exploratory phase[13]. Thus, IBD is still considered as an incurable disease. The goal of treatment in IBD is to suppress intestinal inflammation, ultimately relieving the symptoms and improving the quality of life. UC and CD are heterogeneous diseases and the therapeutic requirements vary among patients. However, there is limited capacity to predict disease progression in individual patients. Therefore, the disease activity and distribution of IBD are taken into account when deciding on the appropriate treatment strategy[25, 26]. Given the known risk of disease progression in IBD, it is important to monitor

for active disease and optimize treatment plans accordingly. Monitoring is essential for identifying disease flares and after introduction of a new therapy[27]. Beyond clinical assessment, objective assessment of disease activity in IBD is essential for guiding subsequent therapy[28]. Classification based on disease severity is also clinically relevant because disease severity is a crucial aspect in most of the current therapeutic algorithms. There are multiple domains of disease activity and severity assessment in IBD, and although each has its merits, none are perfect.

Endoscopy is currently the standard of care in IBD (along with histology) for assessing both disease extent and activity[29]. Clinical remission does not seem to correlate well with inflammation remission at the tissue level. For UC, the Ulcerative Colitis Endoscopic Index of Severity (UCEIS) is the only validated endoscopic index[30, 31]. However, it is associated with some drawbacks: 1) disease extent is not documented, 2) definition of mucosal healing is lacking, and 3) validated thresholds for mild, moderate, or severe disease are also lacking[28]. For CD, the Crohn's Disease Endoscopic Activity Index of Severity (CDEIS) is the most widely used index[32]. While it is validated and reproducible, it is

complex (over 30 entries) and its use may be laborious in actual practice. Additionally, endoscopic evaluation may not always be feasible and it has several limitations related to invasiveness, procedure-related discomfort, inconvenience of extensive bowel cleansing required for an optimal examination, risk of bowel perforation, and relatively poor patient acceptance. A non-invasive technique for evaluating IBD would be desirable as an alternative.

Imaging techniques are non-invasive adjunctive methods to endoscopic assessment. Magnetic resonance imaging (MRI) and bowel ultrasonography (US) demonstrate good sensitivity for assessment of extent and activity of UC, especially when endoscopic evaluation is not feasible[33]. However, these are not yet fully validated in assessing disease activity and there is a delayed timeline as compared to clinical or endoscopic changes[33]. Accuracy may be dependent on the disease site and the examiner[34]. Imaging also has an important role in assessing disease activity in CD because transmural inflammation may be beyond the reach of endoscopy[33], and US and MRI can assess luminal disease activity. Although US may be helpful in evaluating disease activity in CD, its usage

is limited by the availability of an experienced bowel sonographer. MRI has a high diagnostic accuracy for suspected CD and for the evaluation of disease activity and extent. Compared to US, it is less dependent on disease location and the examiner. The Magnetic Resonance Index of Activity (MaRIA), the best-validated index for evaluation of disease activity in CD[35], correlates well with the CDEIS score and is reliable for assessing response to therapy. However, correlation between overall MaRIA and overall CDEIS was not significant at baseline[36]. In diagnosing mild lesions, the accuracy of MRI may be inferior to that of endoscopy[37]. Whether the MRI measures of inflammatory alterations (such as wall thickness, enhancement, edema, ulceration, and diffusion) are responsive to therapy is yet to be determined[38]. Preparations with oral contrast and water enema are required.

Currently, [^{18}F]fluorodeoxyglucose ([^{18}F]FDG) is the most widely used positron emission tomography (PET) tracer for imaging inflammation. The rationale for employing this modality in IBD is an increasing recognition that inflammatory cells display hypermetabolic features due to an up-regulation of glucose transporters to meet the increased metabolic demands in the inflamed state. However, although several positive results have

been published on the utility of [^{18}F]FDG in IBD[39-41], a major limitation is that there is gradual physiologic uptake in the bowel, especially the large bowel[42]. Large patient studies to support the use of this imaging modality for diagnosis and therapy evaluation in IBD are yet to be performed[40, 41].

The system x_C^- is an amino acid antiporter that is composed of a light chain, xCT, and a heavy chain, 4F2hc. It functions in the body by mediating cellular uptake of cystine, which is intracellularly reduced to cysteine for glutathione synthesis (thus protecting cells from oxidative stress[43]) and is extracellularly released (subsequently maintaining a cystine:cysteine redox balance[44]). Several lines of evidence suggest that system x_C^- may play a role in both innate and adaptive immune systems. Prominent upregulation of system x_C^- was observed in activated macrophages and leukocytes[45, 46]. This may be an auto-protecting mechanism from the high levels of reactive oxygen species ('respiratory burst' by macrophages and granulocytes), reducing them through glutathione synthesis. Activation of T cells has been reported to involve expression of system x_C^- not only in antigen presenting cells[47-49] but also in T cells themselves[50, 51]. This allows lymphocytes to take up cysteine at an

activated state. During activation and differentiation of B cells, upregulation of xCT and increased production and release of glutathione and cysteine are also reported[52]. Interestingly, peripheral leukocytes, thymus, spleen, and lymph nodes in humans express very low or absent xCT[53]. All these suggest that system x_C^- is a key player in inflammation.

(4S)-4-(3-^{18}F-fluoropropyl)-L-glutamate (herein referred to as [^{18}F]FSPG) is a new ^{18}F-labeled L-glutamate derivative that is specifically taken up by the system x_C^-[54]. An exploratory clinical study of [^{18}F]FSPG in patients with inflammatory lesions found that [^{18}F]FSPG PET identified inflammatory lesions in all 10 patients and detected all 24 reference lesions[55]. Immunohistochemical (IHC) staining of xCT correlated significantly with that of CD68 while the maximal standardized uptake value (SUV) of [^{18}F]FSPG and staining of CD163 were negatively correlated with a borderline significance. These may indicate that high [^{18}F]FSPG uptake might represent an active disease state by measuring xCT transporter activity in activated M1 macrophages. These results suggested the potential diagnostic value of [^{18}F]FSPG PET to assess the system x_C^- activity in inflammation, particularly in the active stage. [^{18}F]FSPG PET may prove to be useful when [^{18}F]FDG PET

assessment is challenging because of physiologic uptake in normal organs. The very low background, especially in the bowel, should allow for sensitive inflammation imaging[56], especially in IBD. Sulfasalazine, which is routinely used in treating IBD (particularly UC)[57], is a well-known xCT-specific inhibitor[58]. [^{18}F]FSPG PET may also have future potential in selecting patients with high likelihood of responding to sulfasalazine.

The aim of the present study was to assess the feasibility of [^{18}F]FSPG PET in detecting inflammation in murine models of colitis. Another objective was to explore whether [^{18}F]FSPG PET is also useful for assessing disease activity by performing quantitative analyses of [^{18}F]FSPG uptake and comparing the results with clinical and histological markers of disease activity. In addition, expression levels of xCT, Glut1, and immune cell markers were evaluated through IHC to identify their correlations with [^{18}F]FSPG uptake.

Murine models of IBD were employed to predict the feasibility of [^{18}F]FSPG as a useful imaging agent in humans before the actual clinical study. Two different models with confirmed utility in preclinical studies of human IBD were chosen to provide insights into

more than one aspect of IBD, although no single model captures its complexity. Models representing the acute (dextran sodium sulfate [DSS]-induced colitis model) and chronic (T cell-transferred colitis model) stages of IBD were selected[59]. DSS-induced colitis represents the more acute and faster induction of colonic tissue damage and is frequently used to explore the role of innate immune mechanisms in colitis, maintaining epithelial integrity, and studying colon cancer in relation to UC[60]. It is also often used in studying UC because, like in UC, inflammation usually occurs in the left-side colon and epithelial barrier breakdown is prominent[61]. Although to a lesser degree than in UC, the mucus barrier is also affected and intestinal permeability is increased in CD[23, 62]. The T cell transfer model, which involves the complex interplay between innate and adaptive immune mechanisms, represents a chronic model of IBD. It has the advantage of high reproducibility of T cell-dependent chronic intestinal inflammation[63]. Transfer of naïve T cells induces both colitis and small bowel inflammation, making this a model similar to CD[64].

Materials and methods

Ethics Statement

All animal experiments were approved by the Institutional Animal Care and Use Committee of the Asan Biomedical Research Center (Approval No: PN 2017-12-153). Mice were maintained in accordance with the Institutional Animal Care and Use Committee guidelines of the Asan Institute for Life Science. All efforts were made to minimize suffering and experiments were performed under anesthesia with a mixture of ketamine (100 mg/kg) and xylazine (20 mg/kg).

Study design

DSS-induced colitis model

BALB/c mice were administered 5% DSS and underwent PET scanning on day 8 after DSS administration. Daily monitoring was performed to determine the clinical disease activity index (DAI). Development of at least 6 mice with DSS-induced colitis and 6 controls was originally planned. The actual number of mice that developed DSS-induced colitis was 12

and all were included in the analysis. Among these, 6 underwent [^{18}F]FSPG PET/MRI first and then underwent [^{18}F]FDG PET/MRI on the following day while the remaining 6 underwent [^{18}F]FDG PET/MRI first. This was done to ensure that the sequence of [^{18}F]FSPG and [^{18}F]FDG PET/MRIs did not influence radiotracer uptake. After sacrifice, pathologic scoring was performed in a blinded fashion.

Six age- and sex-matched BALB/c mice that received drinking water alone were used as controls. Three mice underwent [^{18}F]FSPG PET/MRI first while 3 underwent [^{18}F]FDG PET/MRI first. Pathologic scoring was performed in a blinded fashion after sacrifice.

IHC staining was performed in a separate group of mice. Colonic tissues that were obtained from 3 BALB/c mice administered 5% DSS and 3 control mice were immunohistochemically stained.

T cell-transferred colitis model

$CD4^{+}CD45RB^{high}$ T cells were transferred into $Rag2^{-/-}\gamma c^{-/-}$ mice. Daily monitoring was performed to determine the clinical disease activity index (DAI). Mice underwent scanning

at approximately 8 weeks after T cell transfer, when clinical signs of colitis were present. Development of at least 6 T cell-transferred mice with colitis and 6 controls was originally planned. The actual number of mice that developed colitis after T cell transfer was 11 and all 11 mice were included in the analysis. Five mice underwent [^{18}F]FSPG PET/MRI first while 6 underwent [^{18}F]FDG PET/MRI first. After sacrifice, pathologic scoring was performed in a blinded fashion.

Ten age- and sex-matched Rag2$^{-/-}$γc$^{-/-}$ mice were used as controls. Five mice underwent [^{18}F]FSPG PET/MRI first while the other 5 underwent [^{18}F]FDG PET/MRI first. Pathologic scoring was performed in a blinded fashion after sacrifice.

IHC staining was performed in a separate group of mice. Colonic tissues that were obtained from 3 T cell-transferred mice and 3 control mice were immunohistochemically stained.

Experimental animals

DSS-induced colitis model

Male BALB/c mice were purchased from Central Lab Animal, Inc. (Seoul, Korea). All mice were maintained under specific pathogen-free conditions in the animal facility at the Asan Biomedical Research Center (Seoul, Korea) where they received sterilized food and water *ad libitum.*

BALB/c mice were treated with 5% DSS (w/v) (MP Biomedicals, Solon, OH) in drinking water *ad libitum* for seven days, followed by one day of normal drinking water. Body weight, rectal bleeding, and diarrhea were monitored daily. DAI was determined as the average of the following scores: weight loss (0, none; 1, 1%-5%; 2, 5%-10%; 3, 10%-20%; 4, >20%), stool consistency (0, normal; 2, loose; 4, diarrhea), and bleeding (0, absence; 2, hemoccult positive; 4, gross bleeding)[65]. Twelve BALB/c mice developed clinical signs of colitis at the time of PET scanning.

Six age- and sex-matched BALB/c mice received drinking water alone and did not show any clinical signs of colitis at the time of PET scanning.

T cell-transferred colitis model

Male Rag2$^{-/-}$γc$^{-/-}$ mice (BALB/c background) were purchased from Jackson Laboratory (Bar

Harbor, ME). All mice were maintained under specific pathogen-free conditions in the animal facility at the Asan Biomedical Research Center (Seoul, Korea) where they received sterilized food and water *ad libitum.*

$CD4^+$ T cells were isolated from spleens of BALB/c mice and purified using a $CD4^+$ T cell isolation kit (Miltenyi Biotech, Bergisch Gladbach, Germany) followed by staining with anti-CD4 (RM4-5) and anti-CD45RB (16A) antibodies (BD Biosciences, Franklin Lakes, NJ). $CD4^+CD45RB^{high}$ T cells (naïve T cells) were sorted on a FACS Aria sorter (BD Biosciences). $Rag2^{-/-}\gamma c^{-/-}$ mice of BALB/c background were injected i.p. with 5×10^5 $CD4^+CD45RB^{high}$ T cells. Body weight and diarrhea were monitored twice a week. DAI was determined based on the following parameters: weight loss (0, none; 2, 5%-15%; 4, >15%) and stool consistency (0, normal; 2, loose; 4, diarrhea)[66]. Eleven $Rag2^{-/-}\gamma c^{-/-}$ mice developed clinical signs of colitis at the time of PET scanning.

Ten age- and sex-matched $Rag2^{-/-}\gamma c^{-/-}$ mice did not receive any T cell transfer and did not show any clinical signs of colitis at the time of PET scanning.

Experimental procedures

A. Imaging

Radiopharmaceutical preparation

Radiolabeling of [^{18}F]FSPG was performed as described previously[55]. [^{18}F]FSPG was batch-manufactured with an automated module (TracerLab MX; GE Healthcare) at Asan Medical Center. Each batch met the in-center criteria in terms of identity, clarity, purity, radioactive concentration, specific activity, pH, sterility, and bacterial endotoxin level. The final product was formulated for injection with a substance per injected unit of 7.4 MBq (0.2 mCi) of [^{18}F]FSPG and 9 nmol or less.

PET/MRI procedure

After fasting (> 12 hours), all mice underwent PET/MRI for two consecutive days ([^{18}F]FSPG PET/MRI on the first day and [^{18}F]FDG PET/MRI on the second day, or vice versa), using the nanoScan PET/MRI system (MEDISO, Hungary).

At 60 minutes after injection through the tail vein (7.4 MBq, i.e., 0.2 mCi of either [^{18}F]FSPG or [^{18}F]FDG), whole body MR imaging was performed using a T1-weighted

gradient-echo (GRE) 3D sequence (TR = 25 ms, TE_{eff} = 3.4, FOV = 64 mm, matrix = 256×256). Ten minutes of static PET scans were acquired with a 1-5 coincident in a single field of view.

Body temperature was maintained by heating air on the animal bed (Multicell Mediso, Hungary) and a pressure sensitive pad was used for respiratory triggering. PET images were reconstructed by Tera-Tomo 3D in full detector mode with all the corrections on, normal regularization, and 4 iterations.

Analysis of PET images

PET images were qualitatively and quantitatively assessed by a board-certified nuclear medicine physician. Multiple volumes of interest were manually drawn along the whole colon loop for the generation of SUV and the highest value in each mouse was chosen for analysis. SUV was calculated using the following formula:

SUV = (tissue radioactivity in the volume of interest measured as MBq/cc x body weight) / injected radioactivity.

***B.* Pathology**

Hematoxylin-eosin (H&E) staining

The entire colon was cut longitudinally and washed vigorously. Colon tissues were then fixed in 4% paraformaldehyde (PFA), embedded in paraffin, and stained with hematoxylin-eosin (H&E).

IHC staining

The entire colon was cut longitudinally and washed vigorously. Colon tissues were then fixed in 1% PFA and dehydrated in 15% sucrose in phosphate-buffered saline (PBS) overnight at 4°C, and in 30% sucrose for 4 hours at room temperature. Tissues were then embedded in optimal cutting temperature compound (OCT compound) and sections were fixed with acetone at -20°C for 5 min. Slides were blocked with PBS containing 1% bovine serum albumin (BSA) for 1 hour at room temperature and stained with primary antibodies overnight at 4°C. Tissues were washed in PBS, incubated with secondary antibodies at room temperature for 1 hour, and stained with 4′,6-diamidino-2-phenylindole (DAPI, Thermo, Waltham, MA) for 2 min at room temperature followed by mounting with PermaFluor mountant (Thermo, Waltham, MA). Images were captured on an LSM 710 confocal

microscope (Carl Zeiss, Oberkochen, Germany). Primary antibodies were: Alexa Fluor 488-conjugated anti-Glut1 (EPR3915), rabbit anti-xCT, hamster anti-CD11c (HL3), PE-conjugated anti-CD3 (17A2), PE-conjugated anti-F4/80 (CI:A3-1), and PE-conjugated anti-B220 (RA3-6B2). Secondary antibodies were: Alexa Fluor 568 goat anti-hamster IgG, Alexa Fluor 647 donkey anti-rabbit IgG. Antibodies from BD Biosciences, BioLegend (San Diego, CA), Abcam (Cambridge, UK) or Novus Biologicals (Littleton, CO) were used for analysis.

Pathologic scores

Pathologic scoring of the DSS-induced colitis model was performed in a blinded fashion using a scoring system described previously[67]. In brief, three parameters were measured: severity of inflammation (0, none; 1, slight; 2, moderate; 3, severe), extent of injury (0, none; 1, mucosa; 2, mucosa and submucosa; 3, transmural and epithelium lost), and crypt damage (0, none; 1, basal one-third damaged; 2, basal two-thirds damaged; 3, only surface epithelium intact; 4, entire crypt and epithelium lost). The sum of the three parameter values was multiplied by a factor that reflected the percentage of tissue involvement (1, 0-25%; 2, 26-50%, 3, 51-75%; 4, 76-100%).

Pathological analysis of the T cell-transferred colitis model was performed using the following scoring criteria[66]: (1) crypt architecture (0, normal; 1, irregular; 2, moderate crypt loss [10-50%]; 3, severe crypt loss [50-90%]; 4, small/medium sized ulcers [< 10 crypt widths]; 5, large ulcers [> 10 crypt widths]); (2) crypt abscesses (0, normal; 1, 1-5; 2, 6-10; 3, >10); (3) tissue damage (0, normal; 1, discrete lesions; 2, mucosal erosions; 3, extensive mucosal damage); (4) inflammatory cell infiltration (0, occasional infiltration; 1, increased leukocytes in lamina propria; 2, confluence of leukocytes extending to submucosa; 3, transmural extension of inflammatory infiltrates); and (5) goblet cell loss (0, normal and < 10% loss; 1, 10-25%; 2, 25-50%; 3, > 50%). The total pathological score was calculated by combining the scores for each of the five parameters, with a maximum score of 17.

Statistical analysis

Development of at least 6 mice for each experimental and control group was originally planned, with an eventual production of 12 DSS-induced colitis mice (and 6 controls) and 11 T cell-transferred colitis mice (and 10 controls). Mann-Whitney *U* tests were performed to

compare variables between groups. Correlations were calculated with the nonparametric Spearman's rho test. All statistical analyses were performed using the statistical software package SPSS 21.0 (SPSS Inc., IBM Company). $P < 0.05$ was considered statistically significant.

Results

Murine colitis models

DSS-induced colitis model

After DSS administration for 7 days, body weight loss was observed in DSS-treated mice. The DAI, including weight loss, stool consistency, and bleeding, was significantly higher in DSS-treated mice than in the control mice ($p < 0.001$, Figure 1A). The shortening of colon length, which has proven to be a useful marker of colitis[68], was also observed in DSS-treated mice ($p < 0.001$, Figure 1B). The pathologic score derived from colon tissues was significantly higher in DSS-treated mice than in control mice ($p = 0.001$, Figure 1C). These results are also presented in Table 1.

T cell-transferred colitis model

As reported previously[64], body weight loss and diarrhea in $Rag2^{-/-}\gamma c^{-/-}$ mice were observed around 6-8 weeks after $CD4^{+}CD45RB^{high}$ T cell transfer (Figure 2A). At the time of sacrifice, the DAI was significantly higher in the T cell-transferred $Rag2^{-/-}\gamma c^{-/-}$ mice than in control mice ($p < 0.001$, Figure 2B). The pathologic score was also significantly higher in T cell-

transferred mice than in control mice ($p < 0.001$, Figure 2C). These results are also presented in Table 2.

PET/MRI images

The yield of non-decay-corrected [^{18}F]FSPG was 23.0 ± 4.1% (range, 19.5-27.6%), and the specific activity was 1989.3 ± 688.7 GBq/µmol (range, 821.1-2929.6 GBq/µmol) at the end of synthesis. Its purity was 94.3 ± 2.8% (range, 90.56-95.64%). The actual amount of [^{18}F]FSPG injected was 8.14 ± 0.74 MBq (range, 7.03-9.62 MBq). The amount of [^{18}F]FDG injected was 8.05 ± 0.71 MBq (range, 6.99-9.88 MBq).

[^{18}F]FSPG PET/MRI images were well obtained in all mice. Images were assessed both qualitatively and quantitatively. Uptake in the rectum, which closely abuts the urethra, required careful assessment. However, co-registration of MRI with PET allowed for better anatomical localization than in other animal studies using PET/CT.

DSS-induced colitis model

By visual assessment of [^{18}F]FSPG PET, DSS-treated mice exhibited mild uptake along the

colon loop while control mice did not show any significant uptake in the colon. In both groups, there was physiologic [^{18}F]FSPG uptake in the pancreas (where system x_C^- is prominently expressed), kidneys, bladder, and urethra (due to renal excretion), and the background activity was low. On [^{18}F]FDG PET, DSS-treated mice showed mild uptake in the colon.

The SUV measured on [^{18}F]FSPG PET was 2.11 ± 1.01 (range, 0.52-3.92) and 0.93 ± 0.49 (range, 0.54-1.85) in the DSS-treated and control mice, respectively. There was a significant difference in [^{18}F]FSPG uptake between the two groups (p = 0.02). The sequence of the two different tracer PET scans ([^{18}F]FSPG and then [^{18}F]FDG or vice versa) did not affect the SUV measured on [^{18}F]FSPG PET. SUVs measured on [^{18}F]FDG PET in DSS-treated and control mice were 2.05 ± 1.14 (range 0.80-3.68) and 0.95 ± 0.24 (range 0.56-1.25), respectively, and the differences in [^{18}F]FDG uptake were on the borderlines of significance (p = 0.08) between both groups. The sequence of the two PET scans did not affect the SUV measured on [^{18}F]FDG PET. There was no significant difference between SUV values on [^{18}F]FSPG and [^{18}F]FDG PET in both DSS-treated and control groups.

Representative [^{18}F]FSPG PET images are shown in Figure 3. SUVs measured in each mouse are presented in Table 1.

T cell-transferred colitis model

By visual assessment of [^{18}F]FSPG PET, Rag2$^{-/-}$γc$^{-/-}$ mice with CD4^{+}CD45RB^{high} T cell transfer showed moderate to strong uptake along the colon loop while control mice did not show any significant uptake. Physiologic [^{18}F]FSPG uptake was observed in the pancreas, kidneys, bladder, and urethra, and the background activity was low. On [^{18}F]FDG PET, Rag2$^{-/-}$γc$^{-/-}$ mice with CD4^{+}CD45RB^{high} T cell transfer showed strong uptake in the colon.

SUVs measured on [^{18}F]FSPG PET in T cell-transferred and control mice were 4.51 ± 1.36 (range 2.89-6.82) and 0.69 ± 0.13 (range 0.50-0.93), respectively. There was a significant difference in [^{18}F]FSPG uptake between the two groups (p < 0.001). The sequence of the PET scans did not affect the SUV measured on [^{18}F]FSPG PET. SUVs measured on [^{18}F]FDG PET in T cell-transferred and control mice were 9.82 ± 4.49 (range 3.30-18.82) and 0.91 ± 0.30 (range 0.60-1.62), respectively, and there was a significant difference in [^{18}F]FDG uptake between both groups (p < 0.001). The sequence of the two

PET scans did not affect the SUV measured on [^{18}F]FDG PET. [^{18}F]FDG values were significantly higher than [^{18}F]FSPG SUVs in both T cell-transferred and control groups.

Representative [^{18}F]FSPG PET images are shown in Figure 4. SUVs measured in each mouse are presented in Table 2.

Comparison between models

T cell-transferred colitis models had significantly higher SUVs than DSS-induced colitis models on both [^{18}F]FSPG ($p < 0.001$) and [^{18}F]FDG PET ($p < 0.001$).

Correlation analysis

DSS-induced colitis model

[^{18}F]FSPG uptake showed positive associations with DAI ($\rho = 0.569$, $p < 0.05$) and pathologic score ($\rho = 0.646$, $p < 0.05$). [^{18}F]FDG uptake also showed positive associations with DAI ($\rho = 0.628$, $p < 0.05$) and pathologic score ($\rho = 0.609$, $p < 0.05$).

T cell-transferred colitis model

[^{18}F]FSPG uptake showed positive associations with both DAI ($\rho = 0.738$, $p < 0.05$) and

pathologic score ($\rho = 0.741$, $p < 0.05$). [^{18}F]FDG uptake also showed positive associations with DAI ($\rho = 0.806$, $p < 0.05$) and pathologic score ($\rho = 0.752$, $p < 0.05$).

IHC staining

DSS-induced colitis model

To determine which immune cells are involved in [^{18}F]FSPG and [^{18}F]FDG uptake, we performed IHC staining of xCT (a subunit of the system x_C^-[69]) and Glut1 (glucose transporter 1, which is the main contributor to FDG uptake). As shown in Figure 5 and 6, expression levels of xCT and Glut1 in DSS-treated mice were enhanced in the epithelium and lamina propria of the proximal, middle, and distal regions of colon tissues, while they were detected only in the colonic epithelial surface of control mice. Overall, expressions of xCT and Glut1 showed similar patterns. Numbers of CD11c$^+$ dendritic cells (DC), F4/80$^+$ macrophages, and CD3$^+$ T cells were increased in the colonic lamina propria of DSS-treated mice. CD11c$^+$ DC and F4/80$^+$ macrophages in the colons of DSS-treated mice were highly co-expressing xCT and Glut1. Both xCT and Glut1 were also expressed in some CD3$^+$ T cells in DSS-treated

mice (Figure 6, 7). $B220^+$ B cells in colonic patches of DSS-treated mice expressed similar levels of xCT as those of control mice (data not shown).

T cell-transferred colitis model

As reported previously[64], colon tissues from $Rag2^{-/-}\gamma c^{-/-}$ mice following $CD4^+CD45RB^{high}$ T cell transfer had markedly elongated crypts and greater infiltration of inflammatory cells in the lamina propria. Expressions of xCT and Glut1 in T cell-transferred $Rag2^{-/-}\gamma c^{-/-}$ mice were significantly enhanced in the epithelium of proximal, middle, and distal regions of the colon. Furthermore, there were markedly increased expressions of xCT and Glut1 in the lamina propria regions of the colon (Figure 8, 9). A higher proportion of immune cells expressed xCT than Glut1. Immune cells expressing xCT were more numerous than those in DSS-treated mice. Most $CD11c^+$ cells co-expressed xCT and Glut1, while $F4/80^+$ and $CD3^+$ cells were partially co-expressing xCT and Glut1 in the whole colon from T cell-transferred mice (Figure 9, 10). No $B220^+$ cell was found in the colon tissues of T cell-transferred mice (data not shown). Expressions of xCT and Glut1 were limited to the surface epithelial cells of colon in control $Rag2^{-/-}\gamma c^{-/-}$ mice (Figure 8).

Discussion

[^{18}F]FSPG, the imaging biomarker for system x_C^-, has been relatively unexplored in inflammatory diseases[55]. This is the first study demonstrating that [^{18}F]FSPG PET is a feasible noninvasive modality for detecting inflammation in murine models of colitis. [^{18}F]FSPG showed a favorable distribution pattern as a potential tracer for evaluating IBD, with low background activity, especially in the large bowel. Not only was there significant [^{18}F]FSPG uptake along the colon in both colitis models, but there was also a positive correlation between [^{18}F]FSPG uptake and disease severity (DAI and pathologic score). These data suggest that [^{18}F]FSPG can be used as a noninvasive radiotracer for imaging inflammation in murine colitis.

We proceeded to determine the source of [^{18}F]FSPG uptake and performed IHC analysis. [^{18}F]FSPG uptake is known to be positively correlated with IHC staining of xCT, a subunit of system x_C^-, in tumor cells[69]. Staining for xCT found prominent expression in the epithelium and also in many immune cells. This is in line with the results of previous studies that the induction of inflammation enhances xCT expression in the epithelium[70] and lamina

propria[71] (inflammatory cells[45, 46, 48, 70], including T cells[50, 51]) in various sites including the colon[71]. A previous clinical study assessing inflammatory diseases mainly in the lung attributed [^{18}F]FSPG uptake to classically activated (M1) macrophages[55]. The present study suggests that [^{18}F]FSPG uptake in colitis is not only increased in macrophages, but also in the epithelium and in other immune cells (such as T cells). A previous preclinical study in which turpentine oil was injected into calf muscles in mice demonstrated negligible uptake at the inflammation site at 72 hours post-injection[54]. After turpentine oil injection, the cell population predominantly comprises lymphocytes and neutrophils during the acute phase (day 1-2)[72, 73], which change to cells of the monocyte/macrophage lineage afterwards[74]. At the time of scanning in the above study[54], inflammation may already have passed the active stage. Had the scanning been performed earlier, increased uptake may have been observed because according to the present and previous studies[55], activated lymphocytes as well as M1 macrophages take up [^{18}F]FSPG.

Because a preceding study suggested that [^{18}F]FSPG uptake correlated with activated macrophage activity[55], we first expected to find higher uptake in the DSS-treated

mice, which represent acute damage and innate immune mechanisms. However, T cell-transferred mice had higher [^{18}F]FSPG uptake than DSS-treated mice, which was unexpected. T cell-transferred mice probably had higher uptake because [^{18}F]FSPG uptake in both models was mainly detected in the epithelium and lamina propria, with supplementary uptake in immune cells. T cell-transferred mice are known to present with greatly thickened walls with epithelial hyperplasia, crypt elongation, and proliferation[64, 75, 76], while DSS-induced colitis mice have increased apoptosis and decreased proliferation in the epithelium[61]. In contrast to normal colon tissue, xCT expression is induced in the inflamed mucosal cells in IBD[71]. Furthermore, the fact that a higher proportion of immune cells expressed xCT (compared to DSS-treated mice) also contributed to the higher [^{18}F]FSPG uptake in T cell-transferred mice. T cell-transferred mice developed colitis at approximately 8 weeks after T cell transfer, which probably provided sufficient time for immune cells to express xCT.

The fact that [^{18}F]FSPG PET showed better performance in T cell-transferred mice is promising from the perspective of performing human studies. CD4^{+} T cells, including Th1, Th2, and Th17 subsets, are known chief mediators in IBD[77]. Many experimental studies

suggest that chronic gut inflammation results from a dysregulated immune response to components of the normal gut flora, and it is reasonable to accept that T cell-transferred mice are more relevant to human IBD than the erosive, self-limiting model of DSS-treated mice[16, 64]. Future clinical studies should help establish the role of [^{18}F]FSPG PET in the evaluation of human IBD.

To further validate the utility of [^{18}F]FSPG PET as an imaging tool for inflammatory assessment in IBD, an intra-animal cross-modality comparison was performed. Although several immune-PET tracers have been reported to be useful in the assessment of colitis models[14-17], [^{18}F]FDG PET remains the most well-established tool for the evaluation of murine colitis models and human IBD[78-80]. The cellular source of [^{18}F]FDG uptake in colitis models is a matter of debate; some found that [^{18}F]FDG uptake specifically detects activated T cells[78] while others insist that it is associated with neutrophil infiltration[79, 81]. Taken together, the evolving nature of cell infiltrate (initially neutrophils, then T cells) is probably the cellular source of [^{18}F]FDG[82]. In T cell-transferred mice, a higher proportion of immune cells expressed xCT than Glut1, while expressions were similar in DSS-treated

mice. In chronic colitis, it is likely that immune cell infiltrates are better visualized by [^{18}F]FSPG than [^{18}F]FDG due to the higher expression of the target transporter. Despite this speculation, [^{18}F]FDG uptake was higher than that of [^{18}F]FSPG in T cell-transferred mice. This is probably because [^{18}F]FDG uptake was not only in immune cells, but was mainly in the epithelium and lamina propria. Other conditions such as muscle contraction or cell regeneration may also have contributed[83, 84]. Interestingly, while Glut1 is considerably expressed in mouse colons (at basal side of epithelial cells)[85], it is absent in human colonic epithelium and its expression in the human colon is generally thought to suggest colorectal carcinoma[86]. This suggests that even if [^{18}F]FDG uptake was higher than that of [^{18}F]FSPG in a chronic murine model, human studies may find better performance of [^{18}F]FSPG presuming that epithelial uptake of [^{18}F]FDG is nearly absent. A mild degree of epithelial uptake via Glut2 may still be present because Glut2 and Glut5 are reported to be expressed in the human colonic epithelium[87]. Nevertheless, while the uptake of [^{18}F]FDG in humans is a mixture of peristaltic activity and immune cell uptake, [^{18}F]FSPG uptake will reflect both epithelial and immune cell alterations.

The present study employed PET/MRI, which has the advantage of excellent soft tissue contrast, instead of PET/computed tomography (CT). The acquired images were of high quality, enabling easier anatomical localization than in other studies using PET/CT. Better localization led to accurate measurement of tracer uptake, especially in DSS-treated mice in which uptakes were lower than in T cell-transferred mice.

Conclusion

In conclusion, [^{18}F]FSPG PET is a useful means of evaluating murine models of colitis. Its uptake was higher in the chronic colitis model and was positively correlated with clinical and histological markers of disease activity. [^{18}F]FSPG may be a promising agent for assessing human IBD, especially when [^{18}F]FDG PET assessment becomes challenging because of physiologic colon uptake.

References

1. M'Koma AE. Inflammatory bowel disease: an expanding global health problem. Clin Med Insights Gastroenterol 2013;6:33-47.
2. Panaccione R. Mechanisms of inflammatory bowel disease. Gastroenterol Hepatol (N Y) 2013;9:529-32.
3. Panes J, Jairath V, Levesque BG. Advances in Use of Endoscopy, Radiology, and Biomarkers to Monitor Inflammatory Bowel Diseases. Gastroenterology 2017;152:362-373 e3.
4. Molodecky NA, Soon IS, Rabi DM, et al. Increasing incidence and prevalence of the inflammatory bowel diseases with time, based on systematic review. Gastroenterology 2012;142:46-54 e42; quiz e30.
5. Ghosh S, Mitchell R. Impact of inflammatory bowel disease on quality of life: Results of the European Federation of Crohn's and Ulcerative Colitis Associations (EFCCA) patient survey. J Crohns Colitis 2007;1:10-20.
6. Kassam Z, Belga S, Roifman I, et al. Inflammatory bowel disease cause-specific mortality: a primer for clinicians. Inflamm Bowel Dis 2014;20:2483-92.
7. Rogler G, Biedermann L, Scharl M. New insights into the pathophysiology of inflammatory bowel disease: microbiota, epigenetics and common signalling pathways. Swiss Med Wkly 2018;148:w14599.
8. Roman AL, Munoz F. Comorbidity in inflammatory bowel disease. World J Gastroenterol 2011;17:2723-33.
9. Farraye FA, Melmed GY, Lichtenstein GR, et al. ACG Clinical Guideline: Preventive Care in Inflammatory Bowel Disease. Am J Gastroenterol 2017;112:241-258.
10. Guthrie E, Jackson J, Shaffer J, et al. Psychological disorder and severity of inflammatory bowel disease predict health-related quality of life in ulcerative colitis and Crohn's disease. Am J Gastroenterol 2002;97:1994-9.
11. Xu F, Dahlhamer JM, Zammitti EP, et al. Health-Risk Behaviors and Chronic Conditions Among Adults with Inflammatory Bowel Disease - United States, 2015 and 2016. MMWR Morb Mortal Wkly Rep 2018;67:190-195.

12. Sartor RB. Mechanisms of disease: pathogenesis of Crohn's disease and ulcerative colitis. Nat Clin Pract Gastroenterol Hepatol 2006;3:390-407.
13. Lee HS, Park SK, Park DI. Novel treatments for inflammatory bowel disease. Korean J Intern Med 2018;33:20-27.
14. Bernards N, Pottier G, Theze B, et al. In vivo evaluation of inflammatory bowel disease with the aid of muPET and the translocator protein 18 kDa radioligand [18F]DPA-714. Mol Imaging Biol 2015;17:67-75.
15. Freise AC, Zettlitz KA, Salazar FB, et al. Immuno-PET in Inflammatory Bowel Disease: Imaging CD4-Positive T Cells in a Murine Model of Colitis. J Nucl Med 2018;59:980-985.
16. Dearling JL, Daka A, Veiga N, et al. Colitis ImmunoPET: Defining Target Cell Populations and Optimizing Pharmacokinetics. Inflamm Bowel Dis 2016;22:529-38.
17. Dearling JL, Park EJ, Dunning P, et al. Detection of intestinal inflammation by MicroPET imaging using a (64)Cu-labeled anti-beta(7) integrin antibody. Inflamm Bowel Dis 2010;16:1458-66.
18. Lobaton T, Vermeire S, Van Assche G, et al. Review article: anti-adhesion therapies for inflammatory bowel disease. Aliment Pharmacol Ther 2014;39:579-94.
19. Kim DH, Cheon JH. Pathogenesis of Inflammatory Bowel Disease and Recent Advances in Biologic Therapies. Immune Netw 2017;17:25-40.
20. Lee SH, Kwon JE, Cho ML. Immunological pathogenesis of inflammatory bowel disease. Intest Res 2018;16:26-42.
21. Nemeth ZH, Bogdanovski DA, Barratt-Stopper P, et al. Crohn's Disease and Ulcerative Colitis Show Unique Cytokine Profiles. Cureus 2017;9:e1177.
22. Silva FA, Rodrigues BL, Ayrizono ML, et al. The Immunological Basis of Inflammatory Bowel Disease. Gastroenterol Res Pract 2016;2016:2097274.
23. Matricon J, Barnich N, Ardid D. Immunopathogenesis of inflammatory bowel disease. Self Nonself 2010;1:299-309.
24. Burger D, Travis S. Conventional medical management of inflammatory bowel disease. Gastroenterology 2011;140:1827-1837 e2.
25. Dignass A, Lindsay JO, Sturm A, et al. Second European evidence-based consensus

on the diagnosis and management of ulcerative colitis part 2: current management. J Crohns Colitis 2012;6:991-1030.

26. Dignass A, Van Assche G, Lindsay JO, et al. The second European evidence-based Consensus on the diagnosis and management of Crohn's disease: Current management. J Crohns Colitis 2010;4:28-62.

27. Chang S, Malter L, Hudesman D. Disease monitoring in inflammatory bowel disease. World J Gastroenterol 2015;21:11246-59.

28. Walsh AJ, Bryant RV, Travis SP. Current best practice for disease activity assessment in IBD. Nat Rev Gastroenterol Hepatol 2016;13:567-79.

29. American Society for Gastrointestinal Endoscopy Standards of Practice C, Shergill AK, Lightdale JR, et al. The role of endoscopy in inflammatory bowel disease. Gastrointest Endosc 2015;81:1101-21 e1-13.

30. Travis SP, Schnell D, Krzeski P, et al. Developing an instrument to assess the endoscopic severity of ulcerative colitis: the Ulcerative Colitis Endoscopic Index of Severity (UCEIS). Gut 2012;61:535-42.

31. Travis SP, Schnell D, Krzeski P, et al. Reliability and initial validation of the ulcerative colitis endoscopic index of severity. Gastroenterology 2013;145:987-95.

32. Mary JY, Modigliani R. Development and validation of an endoscopic index of the severity for Crohn's disease: a prospective multicentre study. Groupe d'Etudes Therapeutiques des Affections Inflammatoires du Tube Digestif (GETAID). Gut 1989;30:983-9.

33. Panes J, Bouhnik Y, Reinisch W, et al. Imaging techniques for assessment of inflammatory bowel disease: joint ECCO and ESGAR evidence-based consensus guidelines. J Crohns Colitis 2013;7:556-85.

34. Pascu M, Roznowski AB, Muller HP, et al. Clinical relevance of transabdominal ultrasonography and magnetic resonance imaging in patients with inflammatory bowel disease of the terminal ileum and large bowel. Inflamm Bowel Dis 2004;10:373-82.

35. Rimola J, Ordas I, Rodriguez S, et al. Magnetic resonance imaging for evaluation of Crohn's disease: validation of parameters of severity and quantitative index of

activity. Inflamm Bowel Dis 2011;17:1759-68.

36. Ordas I, Rimola J, Rodriguez S, et al. Accuracy of magnetic resonance enterography in assessing response to therapy and mucosal healing in patients with Crohn's disease. Gastroenterology 2014;146:374-82 e1.

37. Panes J, Bouzas R, Chaparro M, et al. Systematic review: the use of ultrasonography, computed tomography and magnetic resonance imaging for the diagnosis, assessment of activity and abdominal complications of Crohn's disease. Aliment Pharmacol Ther 2011;34:125-45.

38. Van Assche G, Herrmann KA, Louis E, et al. Effects of infliximab therapy on transmural lesions as assessed by magnetic resonance enteroclysis in patients with ileal Crohn's disease. J Crohns Colitis 2013;7:950-7.

39. Perlman SB, Hall BS, Reichelderfer M. PET/CT imaging of inflammatory bowel disease. Semin Nucl Med 2013;43:420-6.

40. Hustinx R. The Utility of FDG PET/CT in Inflammatory Bowel Disease. PET Clin 2012;7:219-25.

41. Saboury B, Salavati A, Brothers A, et al. FDG PET/CT in Crohn's disease: correlation of quantitative FDG PET/CT parameters with clinical and endoscopic surrogate markers of disease activity. Eur J Nucl Med Mol Imaging 2014;41:605-14.

42. Glaudemans AW, de Vries EF, Galli F, et al. The use of (18)F-FDG-PET/CT for diagnosis and treatment monitoring of inflammatory and infectious diseases. Clin Dev Immunol 2013;2013:623036.

43. Lo GG, Ai V, Chan JK, et al. Diffusion-weighted magnetic resonance imaging of breast lesions: first experiences at 3 T. J Comput Assist Tomogr 2009;33:63-9.

44. Banjac A, Perisic T, Sato H, et al. The cystine/cysteine cycle: a redox cycle regulating susceptibility versus resistance to cell death. Oncogene 2008;27:1618-28.

45. Sato H, Fujiwara K, Sagara J, et al. Induction of cystine transport activity in mouse peritoneal macrophages by bacterial lipopolysaccharide. Biochem J 1995;310 (Pt 2):547-51.

46. Sakakura Y, Sato H, Shiiya A, et al. Expression and function of cystine/glutamate transporter in neutrophils. J Leukoc Biol 2007;81:974-82.

47. Angelini G, Gardella S, Ardy M, et al. Antigen-presenting dendritic cells provide the reducing extracellular microenvironment required for T lymphocyte activation. Proc Natl Acad Sci U S A 2002;99:1491-6.

48. Gmunder H, Eck HP, Benninghoff B, et al. Macrophages regulate intracellular glutathione levels of lymphocytes. Evidence for an immunoregulatory role of cysteine. Cell Immunol 1990;129:32-46.

49. Edinger AL, Thompson CB. Antigen-presenting cells control T cell proliferation by regulating amino acid availability. Proc Natl Acad Sci U S A 2002;99:1107-9.

50. Levring TB, Hansen AK, Nielsen BL, et al. Activated human CD4+ T cells express transporters for both cysteine and cystine. Sci Rep 2012;2:266.

51. Siska PJ, Kim B, Ji X, et al. Fluorescence-based measurement of cystine uptake through xCT shows requirement for ROS detoxification in activated lymphocytes. J Immunol Methods 2016;438:51-58.

52. Vene R, Delfino L, Castellani P, et al. Redox remodeling allows and controls B-cell activation and differentiation. Antioxid Redox Signal 2010;13:1145-55.

53. Kim JY, Kanai Y, Chairoungdua A, et al. Human cystine/glutamate transporter: cDNA cloning and upregulation by oxidative stress in glioma cells. Biochim Biophys Acta 2001;1512:335-44.

54. Koglin N, Mueller A, Berndt M, et al. Specific PET imaging of xC- transporter activity using a (1)(8)F-labeled glutamate derivative reveals a dominant pathway in tumor metabolism. Clin Cancer Res 2011;17:6000-11.

55. Chae SY, Choi CM, Shim TS, et al. Exploratory Clinical Investigation of (4S)-4-(3-18F-Fluoropropyl)-L-Glutamate PET of Inflammatory and Infectious Lesions. J Nucl Med 2016;57:67-9.

56. Mosci C, Kumar M, Smolarz K, et al. Characterization of Physiologic (18)F FSPG Uptake in Healthy Volunteers. Radiology 2016;279:898-905.

57. Gan HT, Chen YQ, Ouyang Q. Sulfasalazine inhibits activation of nuclear factor-kappaB in patients with ulcerative colitis. J Gastroenterol Hepatol 2005;20:1016-24.

58. Gout PW, Buckley AR, Simms CR, et al. Sulfasalazine, a potent suppressor of lymphoma growth by inhibition of the x(c)- cystine transporter: a new action for an

old drug. Leukemia 2001;15:1633-40.

59. DeVoss J, Diehl L. Murine models of inflammatory bowel disease (IBD): challenges of modeling human disease. Toxicol Pathol 2014;42:99-110.

60. Kiesler P, Fuss IJ, Strober W. Experimental Models of Inflammatory Bowel Diseases. Cell Mol Gastroenterol Hepatol 2015;1:154-170.

61. Araki Y, Mukaisyo K, Sugihara H, et al. Increased apoptosis and decreased proliferation of colonic epithelium in dextran sulfate sodium-induced colitis in mice. Oncol Rep 2010;24:869-74.

62. McGovern DP, Jones MR, Taylor KD, et al. Fucosyltransferase 2 (FUT2) non-secretor status is associated with Crohn's disease. Hum Mol Genet 2010;19:3468-76.

63. Neurath MF. Animal models of inflammatory bowel diseases: illuminating the pathogenesis of colitis, ileitis and cancer. Dig Dis 2012;30 Suppl 1:91-4.

64. Ostanin DV, Bao J, Koboziev I, et al. T cell transfer model of chronic colitis: concepts, considerations, and tricks of the trade. Am J Physiol Gastrointest Liver Physiol 2009;296:G135-46.

65. Cooper HS, Murthy SN, Shah RS, et al. Clinicopathologic study of dextran sulfate sodium experimental murine colitis. Lab Invest 1993;69:238-49.

66. Eri R, McGuckin MA, Wadley R. T cell transfer model of colitis: a great tool to assess the contribution of T cells in chronic intestinal inflammation. Methods Mol Biol 2012;844:261-75.

67. Dieleman LA, Palmen MJ, Akol H, et al. Chronic experimental colitis induced by dextran sulphate sodium (DSS) is characterized by Th1 and Th2 cytokines. Clin Exp Immunol 1998;114:385-91.

68. Diaz-Granados N, Howe K, Lu J, et al. Dextran sulfate sodium-induced colonic histopathology, but not altered epithelial ion transport, is reduced by inhibition of phosphodiesterase activity. Am J Pathol 2000;156:2169-77.

69. Baek S, Choi CM, Ahn SH, et al. Exploratory clinical trial of (4S)-4-(3-[18F]fluoropropyl)-L-glutamate for imaging xC- transporter using positron emission tomography in patients with non-small cell lung or breast cancer. Clin Cancer Res 2012;18:5427-37.

70. Taguchi K, Tamba M, Bannai S, et al. Induction of cystine/glutamate transporter in bacterial lipopolysaccharide induced endotoxemia in mice. J Inflamm (Lond) 2007;4:20.

71. Sido B, Lasitschka F, Giese T, et al. A prominent role for mucosal cystine/cysteine metabolism in intestinal immunoregulation. Gastroenterology 2008;134:179-91.

72. Hamazawa Y, Koyama K, Okamura T, et al. Comparison of dynamic FDG-microPET study in a rabbit turpentine-induced inflammatory model and in a rabbit VX2 tumor model. Ann Nucl Med 2007;21:47-55.

73. Wu C, Yue X, Lang L, et al. Longitudinal PET imaging of muscular inflammation using 18F-DPA-714 and 18F-Alfatide II and differentiation with tumors. Theranostics 2014;4:546-55.

74. Feghali CA, Wright TM. Cytokines in acute and chronic inflammation. Front Biosci 1997;2:d12-26.

75. Chen YL, Chen YT, Lo CF, et al. Early Detection of T cell Transfer-induced Autoimmune Colitis by In Vivo Imaging System. Sci Rep 2016;6:35635.

76. Belmaati MS, Claesson MH. Depletion of enteroantigen-activated CD4(+) T cells: effects on proliferation and pathogenicity. Int Immunol 2015;27:419-24.

77. Geremia A, Biancheri P, Allan P, et al. Innate and adaptive immunity in inflammatory bowel disease. Autoimmun Rev 2014;13:3-10.

78. Brewer S, McPherson M, Fujiwara D, et al. Molecular imaging of murine intestinal inflammation with 2-deoxy-2-[18F]fluoro-D-glucose and positron emission tomography. Gastroenterology 2008;135:744-55.

79. Hindryckx P, Staelens S, Devisscher L, et al. Longitudinal quantification of inflammation in the murine dextran sodium sulfate-induced colitis model using muPET/CT. Inflamm Bowel Dis 2011;17:2058-64.

80. Chandler MB, Zeddun SM, Borum ML. The role of positron emission tomography in the evaluation of inflammatory bowel disease. Ann N Y Acad Sci 2011;1228:59-63.

81. Dieleman LA, Ridwan BU, Tennyson GS, et al. Dextran sulfate sodium-induced colitis occurs in severe combined immunodeficient mice. Gastroenterology

1994;107:1643-52.

82. Bettenworth D, Reuter S, Hermann S, et al. Translational 18F-FDG PET/CT imaging to monitor lesion activity in intestinal inflammation. J Nucl Med 2013;54:748-55.

83. Wu Y, Li P, Zhang H, et al. Diagnostic value of fluorine 18 fluorodeoxyglucose positron emission tomography/computed tomography for the detection of metastases in non-small-cell lung cancer patients. Int J Cancer 2013;132:E37-47.

84. Lobert P, Brown RK, Dvorak RA, et al. Spectrum of physiological and pathological cardiac and pericardial uptake of FDG in oncology PET-CT. Clin Radiol 2013;68:e59-71.

85. Yoshikawa T, Inoue R, Matsumoto M, et al. Comparative expression of hexose transporters (SGLT1, GLUT1, GLUT2 and GLUT5) throughout the mouse gastrointestinal tract. Histochem Cell Biol 2011;135:183-94.

86. Haber RS, Rathan A, Weiser KR, et al. GLUT1 glucose transporter expression in colorectal carcinoma: a marker for poor prognosis. Cancer 1998;83:34-40.

87. Merigo F, Brandolese A, Facchin S, et al. Glucose transporter expression in the human colon. World J Gastroenterol 2018;24:775-793.

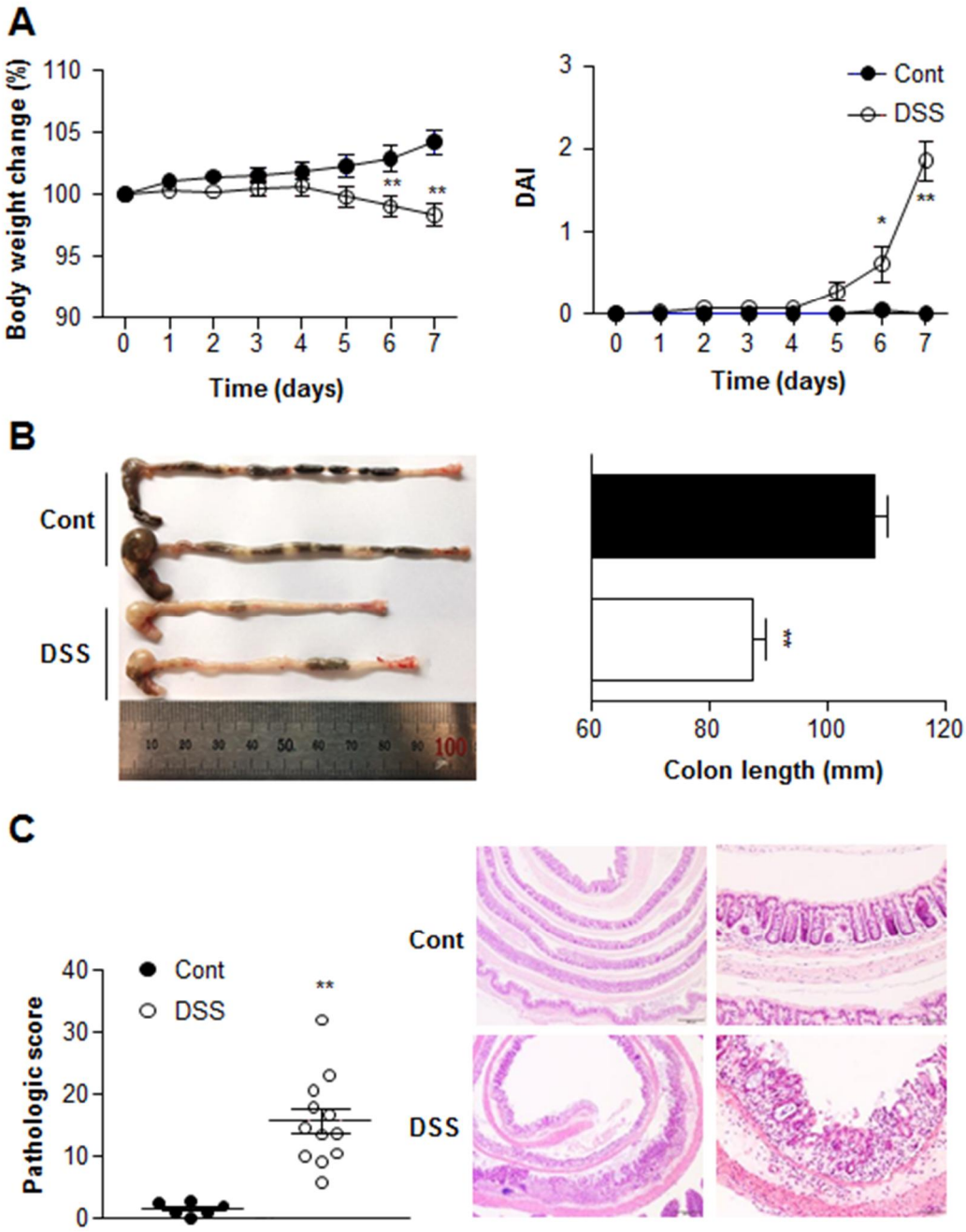

Figure 1. Development of a dextran sodium sulfate (DSS)-induced colitis model. Male BALB/c mice were treated with phosphate-buffered saline (Control group, i.e., Cont, n = 6) or 5% DSS (n = 12) for 7 days. (A) Body weight and disease activity index (DAI), which

were assessed daily, were significantly different between Cont and DSS groups. (B) Colon length measured after sacrifice was significantly shortened in the DSS group. (C) Pathologic scores and representative images of H&E-stained paraffin sections of colon tissue. Pathologic scores were significantly higher in the DSS group. Scale bar = 500 mm. All data are mean ± s.e.m. $*p < 0.05$ $**p < 0.01$

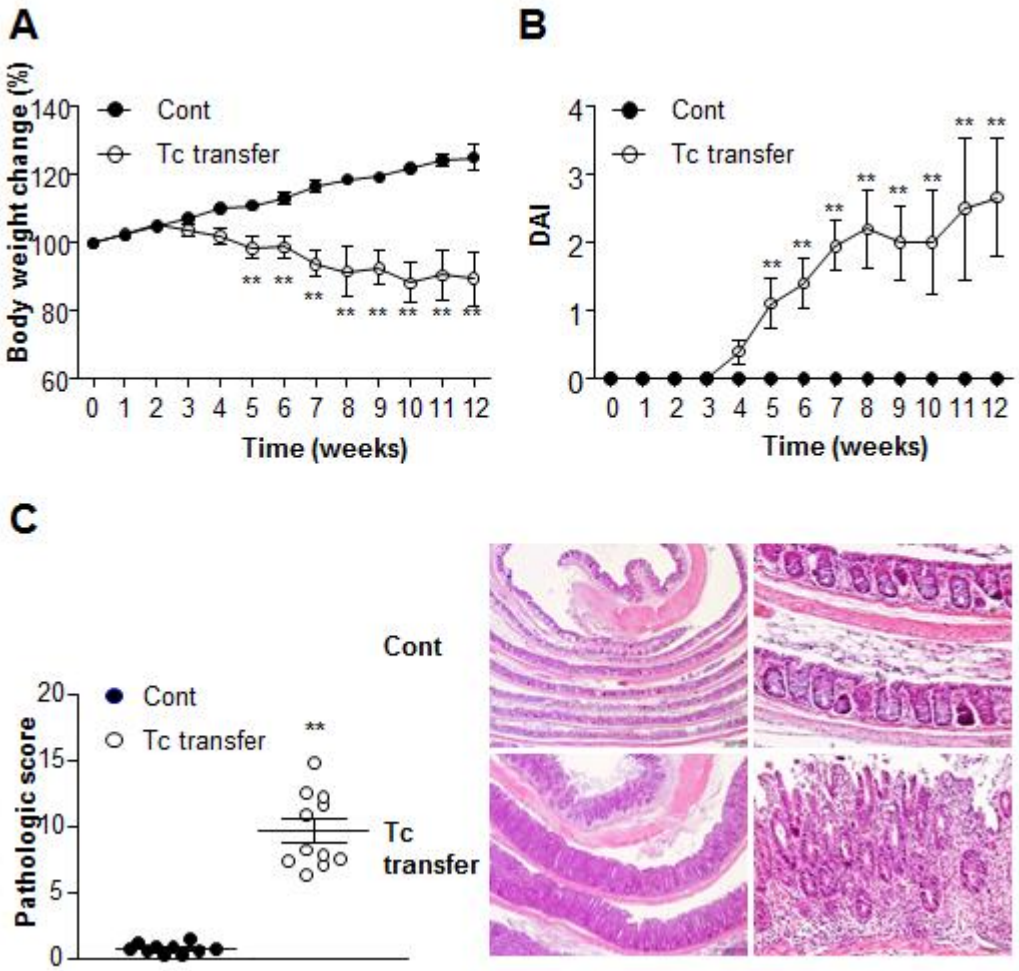

Figure 2. Development of a T cell-transferred colitis model. Rag2$^{-/-}$γc$^{-/-}$ mice of BALB/c background were injected intraperitoneally with phosphate-buffered saline (Control group, i.e., Cont, n = 10) or 5×10^5 CD4$^+$CD45RB^{high} T cells (Tc transfer, n = 11). (A) Body weight and (B) Disease activity index (DAI), which were assessed twice a week, were significantly different between Cont and Tc transfer groups. (C) Pathologic scores and representative images of H&E-stained paraffin sections of colon tissue. Pathologic scores were significantly

higher in the Tc transfer group. Scale bar = 500 mm. All data are mean ± s.e.m. $^{**}p < 0.01$

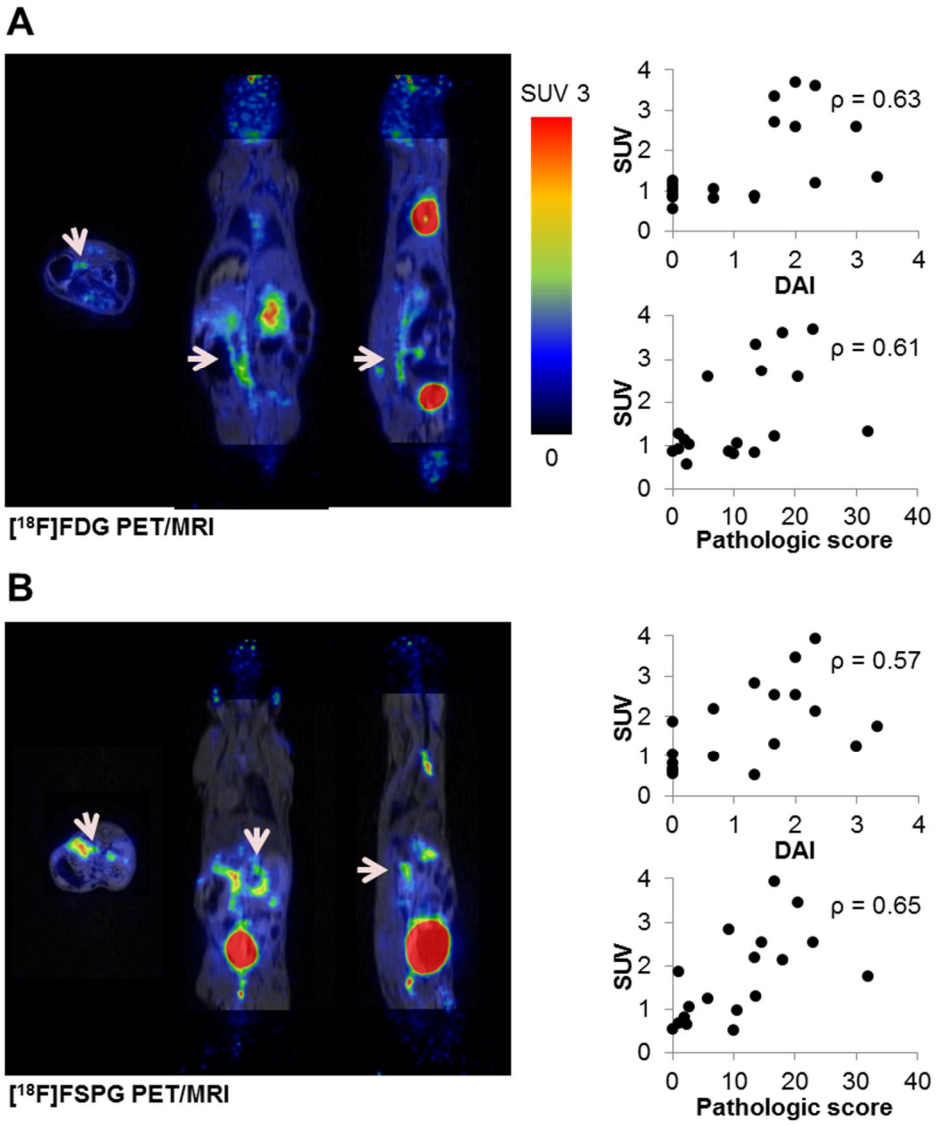

Figure 3. (A) [^{18}F]FDG and (B) [^{18}F]FSPG PET/MRI images of dextran sodium sulfate-treated mice. Representative images show [^{18}F]FDG (A, SUV = 2.7) and [^{18}F]FSPG (B, SUV = 2.5) uptake along the colon on axial, coronal, and sagittal planes. [^{18}F]FDG and [^{18}F]FSPG uptakes both showed positive associations with disease activity index (DAI) and pathologic score. ρ, Spearman's rank correlation coefficient.

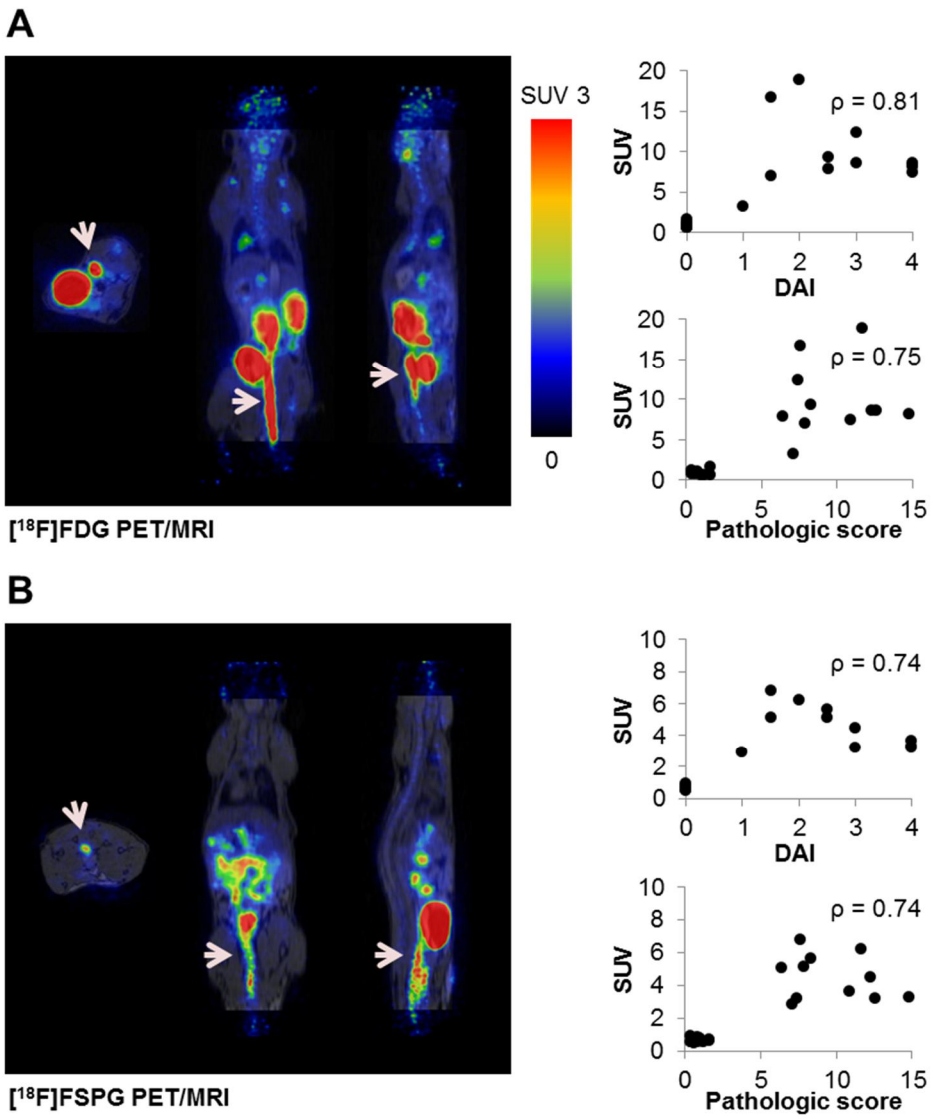

Figure 4. (A) [^{18}F]FDG and (B) [^{18}F]FSPG PET/MRI images of T cell-transferred mice. Representative images show [^{18}F]FDG (A, SUV = 18.8) and [^{18}F]FSPG (B, SUV = 6.2) uptake along the colon on axial, coronal, and sagittal planes. [^{18}F]FDG and [^{18}F]FSPG uptakes both showed positive associations with disease activity index (DAI) and pathologic score. ρ, Spearman's rank correlation coefficient.

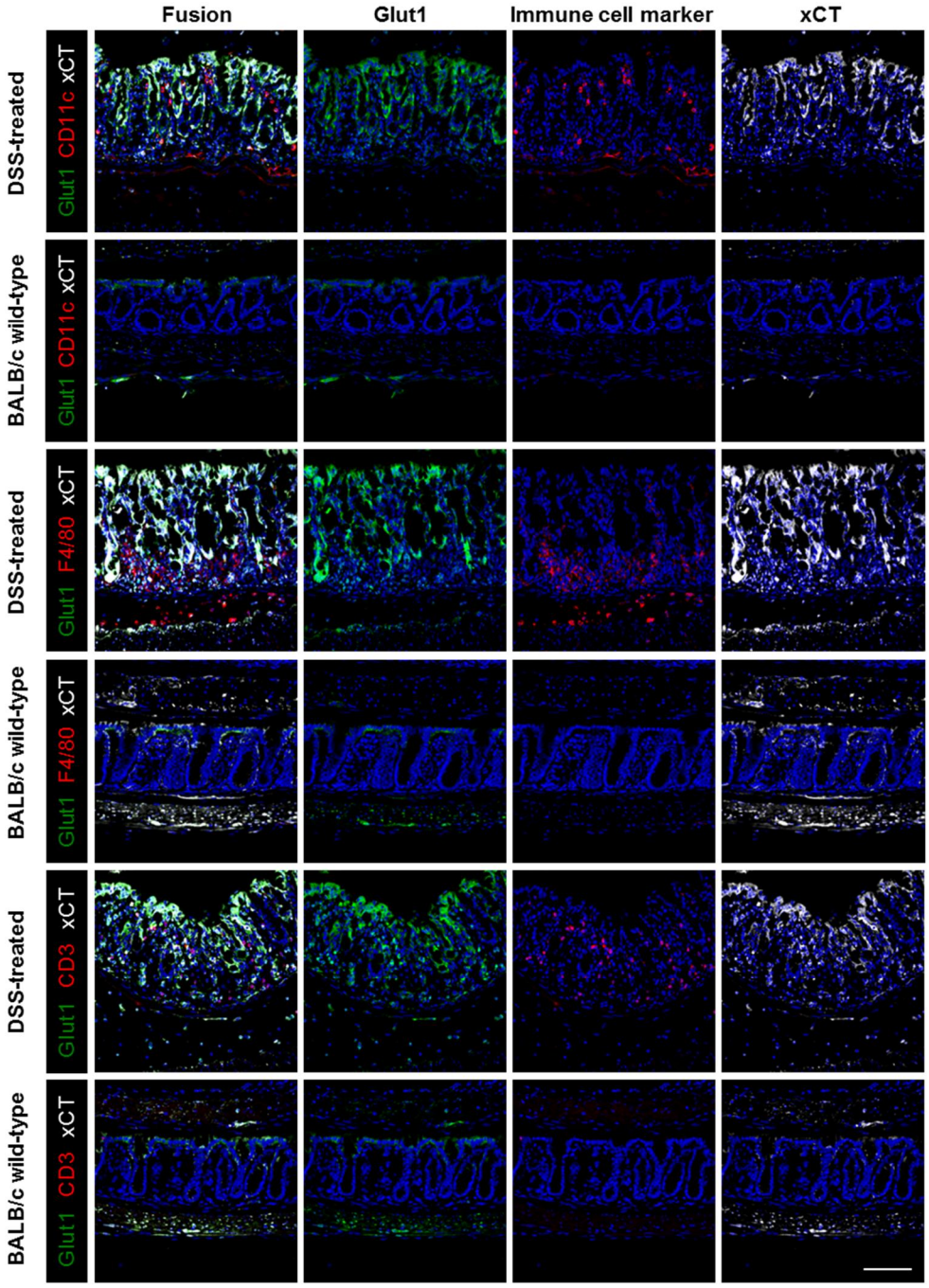

Figure 5. Confocal microscopic images of the middle colon from dextran sodium sulfate (DSS)-treated mice and BALB/c wild-type mice. Images show expressions of xCT (white), Glut1 (green), and immune cells (red). Expressions of xCT and Glut1 in DSS-treated mice

were enhanced in the epithelium and lamina propria. Numbers of $CD11c^+$ dendritic cells, $F4/80^+$ macrophages, and $CD3^+$ T cells were increased in the lamina propria of DSS-treated mice. Primary antibodies: Alexa Fluor 488-conjugated anti-Glut1 (EPR3915), rabbit anti-xCT, hamster anti-CD11c (HL3), PE-conjugated anti-CD3 (17A2), PE-conjugated anti-F4/80 (CI:A3-1), and PE-conjugated anti-B220 (RA3-6B2). Secondary antibodies: Alexa Fluor 568 goat anti-hamster IgG, Alexa Fluor 647 donkey anti-rabbit IgG. Scale bar = 100 μm.

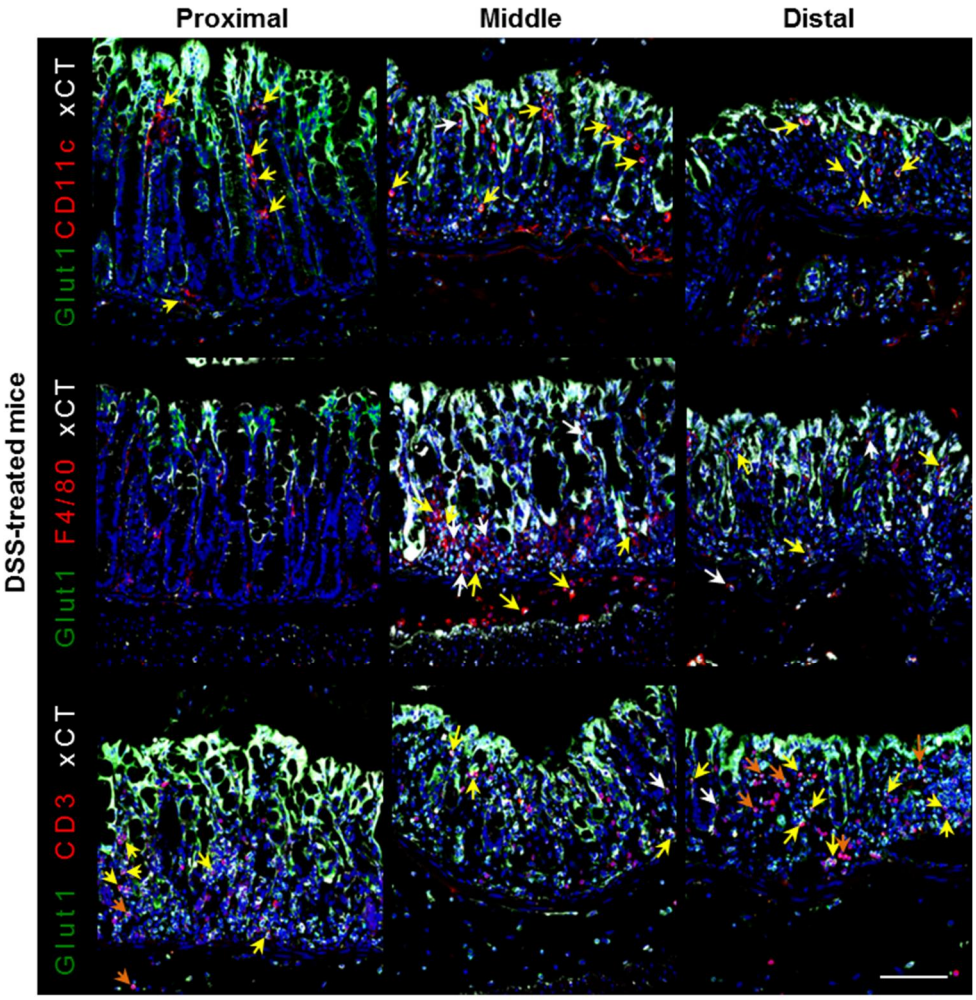

Figure 6. Confocal microscopic images of the proximal, middle, and distal colon from dextran sodium sulfate treated mice. Images show expressions of xCT (white), Glut1 (green), and immune cells (red). Yellow arrows indicate co-expression of xCT, Glut1, and immune cell markers. Orange arrows indicate co-expression of Glut1 and immune cell markers. White arrows indicate co-expression of xCT and immune cell markers. CD11c^{+} dendritic cells and F4/80^{+} macrophages were highly co-expressing xCT and Glut1. Both xCT and

Glut1 were also expressed in some $CD3^+$ T cells. Scale bar = 100 μm.

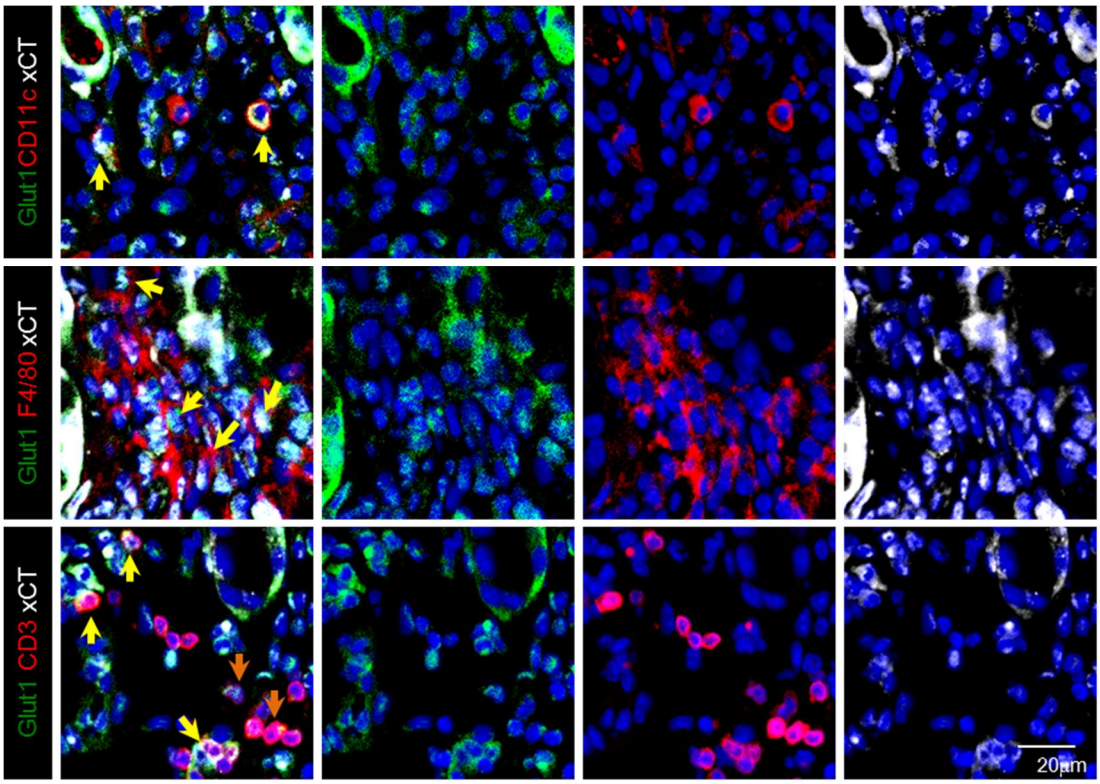

Figure 7. Confocal microscopic images showing cells with co-expressions in the colon from dextran sodium sulfate-treated mice. Images show expressions of xCT (white), Glut1 (green), and immune cells (red). Yellow arrows indicate cells with co-expression of xCT, Glut1, and immune cell markers. Both xCT and Glut1 were co-expressed in $CD11c^+$ dendritic cells, $F4/80^+$ macrophages, and $CD3^+$ T cells. Scale bar = 20 μm.

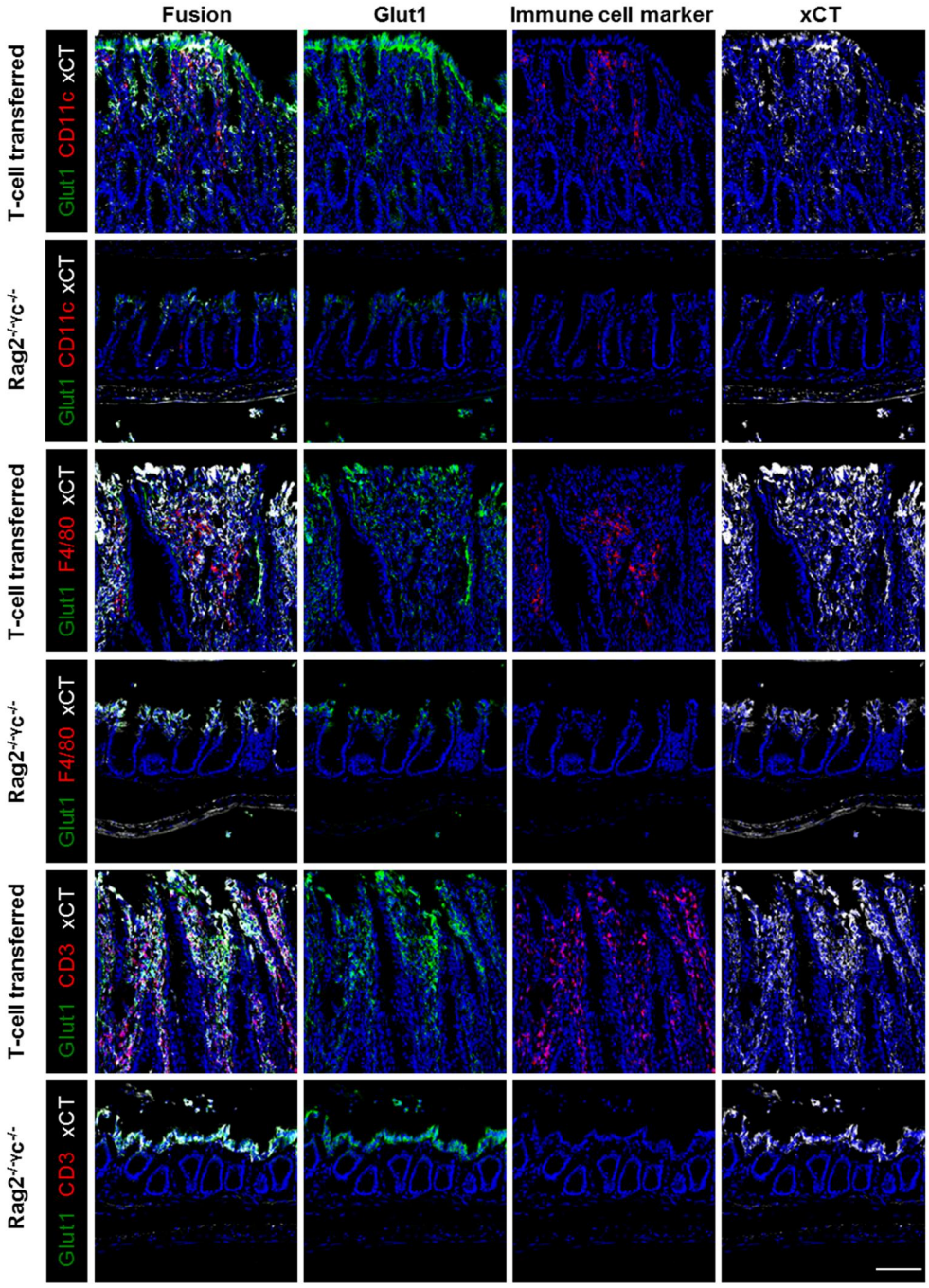

Figure 8. Confocal microscopic images of the middle colon from $CD4^{+}CD45RB^{high}$ T cell-transferred-mice and $Rag2^{-/-}gc^{-/-}$ mice. Images show expressions of xCT (white), Glut1 (green), and immune cells (red). Expressions of xCT and Glut1 in T cell-transferred $Rag2^{-/-}$

$gc^{-/-}$ mice were significantly enhanced in the epithelium and lamina propria. Scale bar = 100 μm.

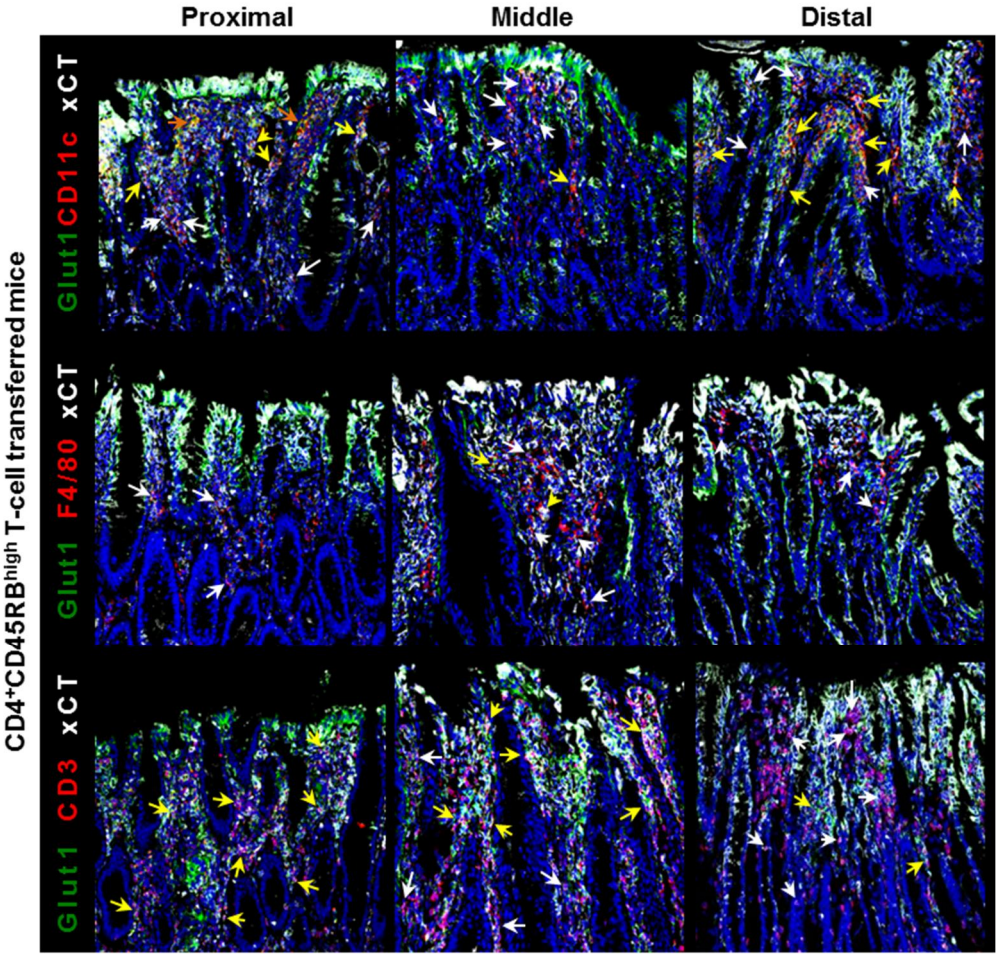

Figure 9. Confocal microscopic images of the proximal, middle, and distal colon from T cell-transferred mice. Images show expressions of xCT (white), Glut1 (green), and immune cells (red). Yellow arrows indicate co-expression of xCT, Glut1, and immune cell markers. Orange arrows indicate co-expression of Glut1 and immune cell markers. White arrows indicate co-expression of xCT and immune cell markers. Most $CD11c^+$ cells co-expressed xCT and Glut1 while $F4/80^+$ and $CD3^+$ cells partially co-expressed xCT and Glut1 in the

whole region of colon. Scale bar = 100 μm.

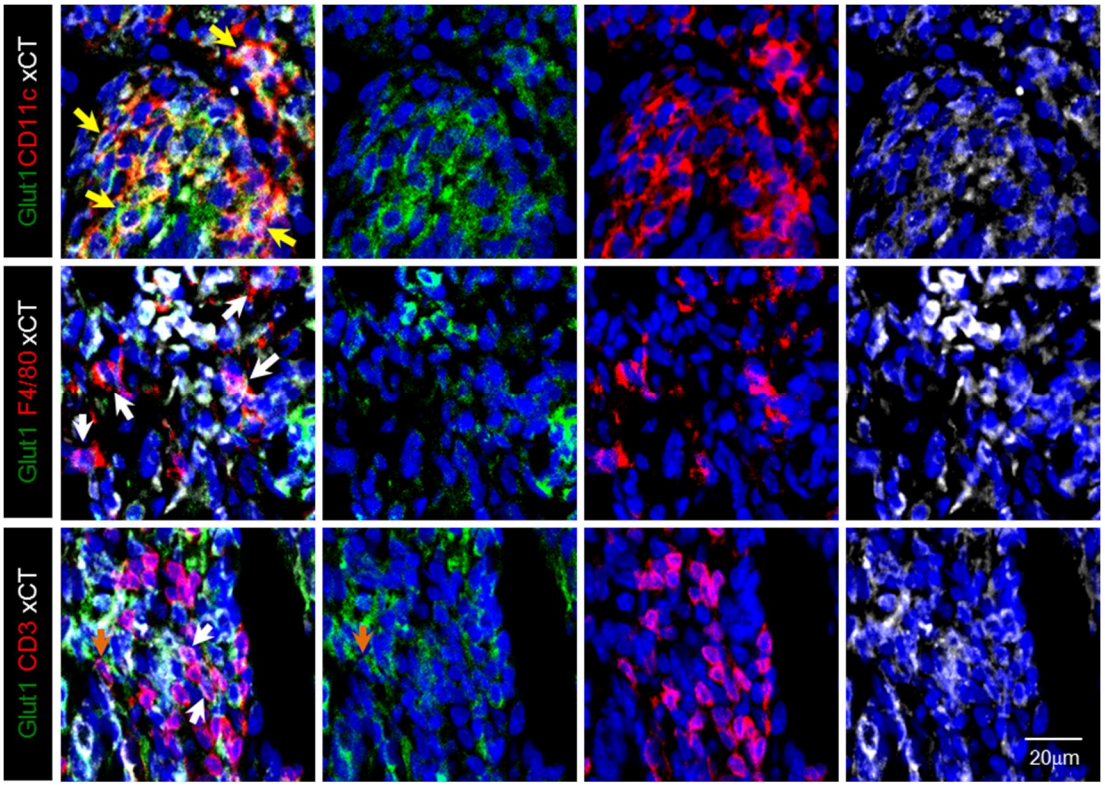

Figure 10. Confocal microscopic images showing cells with co-expressions in the colon from T cell-transferred mice. Images show expressions of xCT (white), Glut1 (green), and immune cells (red). Yellow arrows indicate cells with co-expression of xCT, Glut1, and immune cell markers. Both xCT and Glut1 were co-expressed in $CD11c^{+}$ dendritic cells, $F4/80^{+}$ macrophages, and $CD3^{+}$ T cells. Scale bar = 20 μm.

Table 1. Dextran sodium sulfate (DSS)-treated mice and their controls: Colitis severity and PET findings

Group	No.	DAI*	Colon length (cm)	Pathologic score	FSPG SUV	FDG SUV
Control	1	0	10.8	1.0	1.9	1.3
	2	0	10.5	2.8	1.1	1.0
	3	0	10.6	0.0	0.5	0.9
	4	0	11.5	2.0	0.8	1.1
	5	0	11.5	1.0	0.7	0.9
	6	0	9.5	2.4	0.7	0.6
DSS-treated	1	2.0	7.9	23	2.5	3.7
	2	1.7	8.7	14.7	2.5	2.7
	3	2.0	9.0	20.5	3.5	2.6
	4	2.3	7.7	18.0	2.1	3.6
	5	3.3	8.4	32.0	1.8	1.3
	6	1.7	9.2	13.7	1.3	3.3
	7	0.7	9.7	10.5	1.0	1.1
	8	2.3	9.5	16.7	3.9	1.2
	9	1.3	9.5	9.2	2.8	0.9
	10	0.7	9.2	13.5	2.2	0.8
	11	3.0	8.1	5.8	1.2	2.6
	12	1.3	8.2	10.0	0.5	0.8
P-values †		*<0.001*	*0.001*	*0.02*	*0.02*	*0.08*

*DAI (Disease activity index)

† *P*-values between DSS-treated mice and their controls

Table 2. T cell-transferred mice and their controls: Colitis severity and PET findings

Group	No.	DAI*	Pathologic score	FSPG SUV	FDG SUV
Control	1	0	0.8	0.8	0.9
	2	0	1.0	0.8	0.7
	3	0	1.2	0.6	0.6
	4	0	0.6	0.7	0.9
	5	0	1.6	0.7	0.6
	6	0	0.4	0.6	0.8
	7	0	0.8	0.6	1.0
	8	0	0.6	0.5	0.8
	9	0	1.6	0.7	1.6
	10	0	0.4	0.9	1.2
T cell transfer	1	2.0	11.7	6.2	18.8
	2	3.0	7.4	3.2	12.4
	3	1.0	7.1	2.9	3.3
	4	4.0	14.8	3.3	8.1
	5	4.0	12.6	3.2	8.5
	6	2.5	6.4	5.1	7.9
	7	4.0	10.9	3.6	7.4
	8	1.5	7.6	6.8	16.7
	9	2.5	8.3	5.6	9.3
	10	3.0	12.3	4.5	8.5
	11	1.5	7.9	5.1	7.0
***P-values*†**		*<0.001*	*<0.001*	*<0.001*	*<0.001*

*DAI (Disease activity index)

† *P*-values between T cell-transferred mice and their controls

국문요약

목적 : 본 연구는 (4S)-4-(3-^{18}F-Fluropropyl)-L-Glutamate positron emission tomography/magnetic resonance imaging ([^{18}F]FSPG PET/MRI)를 통하여 대장염 마우스 모델에서의 염증의 발견 가능성을 알아보고자 하였다.

대상 및 방법 : Dextran sodium sulfate (DSS) 투여 또는 T 세포 이식을 통하여 두 종류의 대장염 마우스 모델을 만들었다. 두 모델에서 대장염 증상이 발현된 후 [^{18}F]FSPG 및 [^{18}F]Fluorodeoxyglucose (FDG) PET/MRI 영상들을 획득하였다. 질병활성도 지표(DAI), 조직학적 점수, SUV 를 계산 및 측정하였다. 면역조직화학적 염색을 하여 xCT, Glut1, CD11c, F4/80, CD3, B220 의 발현을 확인하였다.

결과 : 총 12 마리의 DSS 투여 모델과 11 마리의 T 세포 이식 모델에서 대장염이 발생하였다. 두 그룹 모두 대조군과 비교하여 대장에 유의한 [^{18}F]FSPG 섭취를 보였으며, T 세포 이식 그룹의 섭취가 DSS 투여 그룹보다 높았다. T 세포 이식 그룹에서는 [^{18}F]FDG

SUV 가 [^{18}F]FSPG SUV 보다 높았으나 DSS 투여 그룹에서는 유의한 차이가 없었다. [^{18}F]FSPG 섭취는 두 모델에서 모두 DAI, 조직학적 점수와 양의 상관성을 보였다. IHC 염색 결과 두 모델 모두에서 대장의 상피 및 고유판의 xCT 와 Glut1 발현이 유의하게 증가하였다. CD11^{+} 수지상세포, F4/80^{+} 대식세포, CD3^{+} T 세포의 일부에서 xCT 와 Glut1 발현이 증가하였으며, T 세포 이식 그룹에서 염증 세포들의 xCT 발현이 더 높았다.

결론 : [^{18}F]FSPG PET 은 대장염 마우스 모델 평가에 유용한 방법이며, [^{18}F]FSPG 의 섭취는 질병 확성도의 임상적, 조직학적 지표들과 양의 상관성을 보인다. 사람의 염증성 장질환 평가에서의 유용성 여부 확인을 위하여 추가 검사들이 필요할 것이다.

중심 단어 : [^{18}F]FSPG, 양전자단층촬영, 염증성 장질환, 대장염